



Vibrational analysis of pipes based on the drift-flux two-phase flow model

Ali Ebrahimi-Mamaghani^{*}, Navid Mostoufi^{*}, Rahmat Sotudeh-Gharebagh, Reza Zarghami

Multiphase Systems Research Lab., School of Chemical Engineering, College of Engineering, University of Tehran, P.O. Box 11155/4563, Tehran, Iran

ARTICLE INFO

Keywords:

Supported pipe
Two-phase flow
Drift-flux model
Flow mixture velocity
Gas void fraction
Vibrational frequency

ABSTRACT

Linear and nonlinear free vibrations of supported pipes containing two-phase flow were modeled in different flow regimes by including gravitational force, structural and two-phase damping effects. To model the flow, the drift-flux model was utilized. Discretization of the dynamical equation was performed with the help of the Galerkin scheme. The linear vibrational frequency of the system was determined by solving the eigenvalue problem. Also, a mathematical closed-form expression for the nonlinear vibrational frequency is presented. For the validation purpose, theoretical and experimental data were obtained from literature and compared with the results of this work in various operating conditions. A detailed parametric analysis was also carried out to examine the influence of flow parameters, geometry, and physical properties on the dynamics of the system. It was concluded that by increasing the inner and outer pipe diameters, vibrational frequencies of the system decrease and increase, respectively. It was found that a lower liquid phase density leads to an improvement in the vibrational stability of the system. Besides, it was demonstrated that by increasing the void fraction/mixture velocity in the system, linear and nonlinear vibrational frequencies increase/decrease. Furthermore, a higher initial amplitude caused a larger nonlinear frequency shift. The outcomes of the current analysis can be applied as a frame to evaluate and optimize the performance of structures transporting two-phase flows.

1. Introduction

Fluid-conveying pipes are vastly used in chemical plants, offshore production systems, heat exchanger tubes, steam generators, and risers (Paidoussis, 1998; Ye et al., 2021). Hence, prediction of the performance of these pipes from various operational aspects, such as flow pattern (Wiedemann et al., 2019), heat transfer (Zhang and Faghri, 2002), pressure fluctuations (Bi, 2007), and fluid dynamics (Wang and Lyu, 2021), is of interest to engineers, practitioners, and scientists. Considering safety requirements, identifying the dynamical features of transportation pipelines deserves serious attention (Ibrahim, 2011; ElNajjar and Daneshmand, 2020; Xu et al., 2020). The multiphase flow as an excitation mechanism is widely observed in pipes (Oyelade and Oyediran, 2021; Sheikhi et al., 2012). Furthermore, the development of industrial applications is accompanied by new challenges and serious demands for vibrational analysis of piping systems conveying multiphase flows (Montoya-Hernández et al., 2014; Wu et al., 2021). Therefore, profound knowledge and accurate interpretation of the effect of multiphase flow variables on the oscillating pipes are of great importance (Pettigrew and Taylor, 1994a). In the last decades, numerous

efforts have been dedicated to analyzing the induced vibration of two-phase flowing through the pipes (Miwa et al., 2015). Despite the low density of gases, their high compressibility and expandability heighten the complexity of momentum exchange between phases in these structures (Hibiki and Ishii, 1998). In addition, due to the complex and intermittent characteristics of two-phase flows, an in-depth understanding of complicated hydrodynamic phenomena in these systems is crucial for engineers and researchers. Within this context, Monette and Pettigrew (2004) probed the fluidelastic instability of downward cantilevered pipes conveying two-phase flow. They proposed a modified slip-ratio factor by accomplishing several experiments over broad gas void fraction and flow velocity ranges. Charreton et al. (2015) experimentally obtained the damping ratio for pipes conveying two-phase flow. They found that the two-phase damping of the system has a high dependency on the gas void fraction and the flow regime. Based on an experimental study, Sheikhi et al. (2013) simultaneously measured both vibration and pressure in a bubble column. They captured transition points of flow regimes by statistical and frequency analyses. Bamidele et al. (2019) carried out an experimental study on the vibrational behavior of horizontal pipes with flow restricting orifices. They explored

* Corresponding author.

E-mail addresses: a.ebrahimi.mamaghani@gmail.com (A. Ebrahimi-Mamaghani), mostoufi@ut.ac.ir (N. Mostoufi), sotudeh@ut.ac.ir (R. Sotudeh-Gharebagh), r.zarghami@ut.ac.ir (R. Zarghami).

the impact of diverse parameters, such as orifice area ratio, mass quality, and gas void fraction, on the dynamical response of the structure. Zhu et al. (2019) experimentally inspected the slug flow-induced oscillation in flexible curved risers. They acquired vibrational frequency and amplitude of the system in terms of slug flow characteristics and reported the occurrence conditions of the mode-exchange phenomenon in risers.

A comprehensive review of the relevant literature shows that the most available investigations in this subject are categorized within the experiment realm (Pettigrew and Taylor, 1994b). Despite several advantages of analytical models, such as simplicity, repeatability, and low cost, limited studies have been reported on the mathematical modeling of pipes conveying two-phase flows. In this regard, Liu and Wang (2018a) simulated the dynamics of cantilevered pipes conveying two-phase slug flow. By implementing the Galerkin discretization technique, they have computed the fundamental vibrational frequency of the system for various pipe lengths and superficial gas velocities. An and Su (An and Su (2015) conducted the vibrational signature analysis of upward pipes transporting two-phase flows. They solved the dynamical equation of the system by exploiting the generalized integral transform technique and surveyed the influence of gas volumetric flow rate on the vibrational amplitude of the system. Ortiz-Vidal (2019) investigated the dynamical stability of pipes conveying two-phase flow based on different slip-ratio factor models and extracted the critical velocity and frequency of the system. He indicated that at high gas volumetric fractions, the instability threshold of the system is completely dependent on the choice of the slip-ratio. Additionally, he concluded that when the difference between the velocities of gas and liquid is high, applying the homogeneous model fails to assess the stability of the system correctly. Liu and Wang (2018b) presented a theoretical model for the vibration of pipes conveying gas-liquid two-phase slug flow and verified their numerical results by experimental data. They solved the model equation by the finite element method and extracted corresponding superficial gas and liquid velocities to the buckling instability of the system. Carneiro et al. (2011) modeled the vibration of horizontal pipes conveying two-phase slug flow. They reported statistical characteristics of velocity, frequency, and slug length in the system under various operating conditions. Adegoke and Oyediran (2018) analyzed the nonlinear vibration of cantilevered pipes conveying two-phase flow subjected to both axial loading and thermal environment using the multiple-scale method. They revealed that the system stability region shrinks by ascending axial load and temperature rise. Ebrahimi-Mamaghani et al. (2019) considered the divergence and flutter behavior of vertical cantilevered pipes containing two-phase flow incorporating dissipative forces. They discussed the impact of gravity parameter and flow velocity on the time history, Argand diagrams, and stability maps. A probabilistic model for dynamics of horizontal pipes conveying two-phase flow considering uncertainty inflow parameters was established by Ponte et al. (2020). Their results disclosed that variations of flow profile factor and vapor quality remarkably affect the critical velocity, dynamical response, and stochastic behavior of the system. Khudayarov et al. (2019) studied oscillations of composite pipes conveying gas-containing fluids. They addressed the impacts of the tensile force, two-parameter foundation, and viscoelastic properties of the pipe material on the vibration frequency and stability threshold of the system.

Among several two-phase flow models reported in the literature, two distinct fundamental formulations are available to simulate macroscopic field equations of flows: the two-fluid model (TFM) and the drift-flux model (DFM) (Wang et al., 2018). In the TFM, two separate

momentum equitation are considered for each phase. Depending on the degree of the dynamical coupling between the phases, the phase-interaction term plays a crucial role in this model (Ishii and Mishima, 1984). Moreover, because of uncertainty in specifying interfacial interaction terms as well as the possibility of numerical instabilities due to inappropriate choice of these terms, applying the TFM associates with substantial computational difficulties (Goda et al., 2003). On the other hand, compared with the rigorous two-fluid formulation, the DFM is an approximate formulation. In this model, the velocity fields are stated in terms of the drift velocity and the mixture center-of-mass velocity, and consequently, phase-interaction terms are canceled out (Hibiki and Ishii, 2003). The most basic assumption in the DFM is to take into account the mixture as a homogeneous phase instead of two separate phases. In other words, in this model, the dynamics of two phases can be stated by the mixture-momentum equation, and the constitutive kinematic equation considers the relative motion between the two phases. Accordingly, applying the DFM in the formulation of engineering problems, including two-phase flow dynamics, can alleviate difficulties associated with the TFM. It is necessary to mention that other two-phase models are commonly confined to a specific flow regime or require excessive information related to flow patterns, especially in the gravitational flow conditions (Guo et al., 2018). While the DFM based on the gas void fraction correlations provides acceptable consistency over a broad range of operational conditions. Generally, it can be expressed that the DFM is a simple, practical, and fairly accurate model with high computational efficiency for two-phase flow analyses. It is important to mention that when the motions of two phases are strongly coupled, or relative local motion between the phases is significant (e. g., bubbly, finely dispersed bubbly, and churn flow regimes), employment of the DFM is suitable and recommended (Bhagwat and Ghajar, 2014; Hibiki et al., 2004). According to literature and the best of authors' knowledge, despite the practical importance of the DFM in dynamical modeling of structures conveying two-phase flow, the theoretical investigations focused on the cumulative effect of two-phase flow-structure interaction based on the concept of the DFM is sparse. Recently, Li et al. (2020) extended a combined damping model for dynamics of doubly clamped pipes conveying two-phase flow based on the DFM and interpreted the system stability behavior. They addressed the effect of the volumetric gas fraction on the transverse displacement of the system and confirmed that the vibrational amplitude of the system reaches its minimum at the flow transition zone.

It is well known that in engineering applications, internal flow parameters such as gas fraction, mass flux, and two-phase damping, can vary significantly. Since both Coriolis and centrifugal forces arise from the fluid flow, the fluid-structure interaction in pipes conveying two-phase flow changes by variations of physical properties of the internal flow. Therefore, researchers have presented several mechanistic and mathematical models to predict the dynamical behavior and vibrational characteristics of these systems in various operating conditions and flow regimes. The present investigation conducted linear and nonlinear free vibration analyses of restrained vertical pipes conveying gas-liquid two-phase flow in different flow regimes based on the DFM. Also, a parametric study was performed to clarify the relation between flow parameters and induced vibration of supported pipes containing two-phase flow. In the following, the governing dynamical equation of the system incorporating gravitational force, structural and two-phase damping components is presented. Adopting the Galerkin discretization approach, linear and nonlinear vibrational frequencies of the system are then calculated. To verify the presented approach, comparison studies are represented. Finally, the influence of gas void fraction, flow mixture

velocity, boundary conditions, geometrical and physical properties on the system dynamics are evaluated and elucidated.

2. Mathematical formulation

In this section, first, fundamental parameters of two-phase flows are introduced. Afterward, a brief background of the drift flux model is stated. Also, the dynamical equation of the considered model is explained.

2.1. Two-phase flow parameters

The gas void fraction, as an important parameter to describe the two-phase flow behavior, is defined by (Monette and Pettigrew, 2004):

$$\alpha_G = \frac{A_G}{A_C} = \frac{A_G}{A_G + A_L} \quad (1)$$

where A_G and A_L are the areas occupied by gas and liquid phases, respectively, and A_C is the inner cross-sectional area of the pipe. Thus, it follows that:

$$A_G = \alpha_G A_C \quad (2)$$

$$A_L = (1 - \alpha_G) A_C \quad (3)$$

By definition, the gas volumetric fraction is defined as (Monette and Pettigrew, 2004):

$$\varepsilon_G = \frac{Q_G}{Q_G + Q_L} \quad (4)$$

in which Q_G and Q_L are the gas and liquid volumetric flow rates (m^3/s), respectively. It is worth mentioning that the volumetric gas fraction can be estimated by measuring the volumetric flow rates of gas and liquid. Specific instruments, such as fiber optic or capacitance probes, are required to determine the gas void fraction (Charreton et al., 2015).

Velocities of gas and liquid can be expressed, respectively, as follows:

$$U_G = \frac{Q_G}{A_G} \quad (5)$$

$$U_L = \frac{Q_L}{A_L} \quad (6)$$

The flow mixture velocity, as another key parameter of two-phase flow, can be determined as:

$$V = U_{Gs} + U_{Ls} = \frac{Q_G + Q_L}{A_C} \quad (7)$$

where U_{Ls} and U_{Gs} are the liquid and superficial velocities (m/s), respectively.

2.2. Drift-flux model

To model the internal two-phase flow of the system, the drift-flux model is utilized. The drift-flux model has been widely used for formulating the basic equations of multiphase flow in pipelines and annulus, which can be formulated as (Osipov et al., 2014)

$$U_G = C_0 V + U_{GM} \quad (8)$$

in which U_{GM} is the two-phase drift velocity, and C_0 is the distribution parameter. The distribution parameter indicates the distribution of the gas phase across the inner cross-sectional area of the pipe. This parameter reflects the effect of velocity profile and can be considered 1.2 in vertical pipes (Bhagwat and Ghajar, 2012).

It should be stated that according to the steady version of the DFM, it is supposed that the phase change and pressure gradient, which may occur during transient operations such as start-up and shut-down of the

system, are negligible. Also, under the steady-state condition, it is assumed that averaged pressure and stress in the bulk fluid and at the interface are approximately the same (Hibiki and Ishii, 2003).

Based on the DFM, the relationship between flow parameters can be expressed as (Li et al., 2020):

$$\alpha_G = \frac{\varepsilon_G}{C_0 + \frac{U_{GM}}{V}} \quad (9)$$

Bhagwat and Ghajar (2014) compiled several experimental data to distinguish the two-phase flow characteristics. According to the experimental observations, they presented the following flow regime-independent function based on the gas void fraction:

$$U_{GM} = \pm 0.35 \sqrt{\frac{g D_h (\rho_L - \rho_G)(1 - \alpha_G)}{\rho_L}} \quad (10)$$

in which D_h is the hydraulic pipe diameter, and g is the gravitational acceleration. Also, ρ_G and ρ_L are the gas and liquid densities, respectively. It is worth mentioning that positive and negative values of the drift velocity are related to upward- and downward-oriented flows in the system.

Considering that $U_{LS} = U_L(1 - \alpha_G)$, Eq. (7) can be used to obtain the liquid-phase velocity in terms of gas void fraction from:

$$U_L = V - \frac{\alpha_G U_{GM}}{1 - \alpha_G} \quad (11)$$

2.3. Dynamical equation of the model

Fig. 1 shows the schematic view of downward and upward pipes conveying two-phase flow to visualize the considered system better.

The governing nonlinear dynamical equation of vertical pipes transporting gas-liquid two-phase flow with supported, non-sliding ends, including mid-plane stretching effect, is given by (Monette and Pettigrew, 2004; Holmes, 1977):

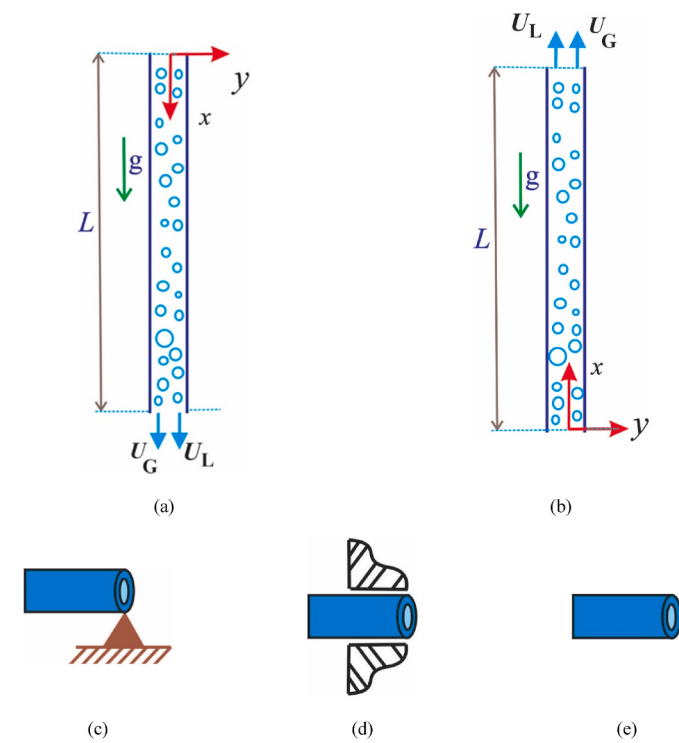


Fig. 1. Architecture of (a) downward and (b) upward pipes conveying two-phase flow with (c) pinned end, (d) clamped end, and (e) free end.

$$EI \left(1 + \frac{\sigma}{\Omega} \frac{\partial}{\partial t} \right) \frac{\partial^4 y}{\partial x^4} \pm (\rho_p A_p + \rho_L A_L + \rho_G A_G) g \left((x - L) \frac{\partial^2 y}{\partial x^2} + \frac{\partial y}{\partial x} \right) \\ + (\rho_L A_L U_L^2 + \rho_G A_G U_G^2 - T) \frac{\partial^2 y}{\partial x^2} + 2(\rho_L A_L U_L + \rho_G A_G U_G) \frac{\partial^2 y}{\partial x \partial t} \\ + c \frac{\partial y}{\partial t} + (\rho_p A_p + \rho_L A_L + \rho_G A_G) \frac{\partial^2 y}{\partial t^2} - \frac{EA_p}{2L} \left(1 + \frac{\sigma}{\Omega} \frac{\partial}{\partial t} \right) \frac{\partial^2 y}{\partial x^2} \int_0^L \left(\frac{\partial y}{\partial x} \right)^2 dx = 0 \quad (12)$$

where E is Young's modulus, I is the moment of inertia, σ is the hysteretic structural damping coefficient, y is the transverse deflection, A_p is the outer cross-sectional area, and Ω is the circular frequency of the pipe. Also, ρ_p is the pipe density, L is the pipe length, T_0 is the initial axial tension force in the pipe, x is the distance from the pipe support, and c is the damping coefficient of the inertial flow.

In Eq. (12), the first term is the elastic restoring force with the structural damping effect, which is a function of the material and supports of the pipe. The second term signifies the gravitational effects on the system. It is important to mention that positive and negative signs for the gravitational force refer to the pipes with downward and upward flow orientations, respectively. The third term is related to centrifugal and tensile forces due to the internal flow and the initial axial tension force. The fourth and fifth terms are related to Coriolis and two-phase damping forces. The last cubic nonlinear term in Eq. (12) is originated from the additional axial load induced by the transverse motion of the pipe (Mou and Bai, 2018). Note that the longitudinal direction of the pipe coincides with the x -axis (along with the gravity orientation).

For the pinned-pinned (P-P), clamped-clamped (C-C), and clamped-free (C-F) systems, the boundary conditions are as follows, respectively:

$$x=0, L : y = \frac{\partial^2 y}{\partial x^2} = 0 \quad (13)$$

$$x=0, L : y = \frac{\partial y}{\partial x} = 0 \quad (14)$$

$$x=0 : y = \frac{\partial y}{\partial x} = 0, x=L : \frac{\partial^2 y}{\partial x^2} = \frac{\partial^3 y}{\partial x^3} = 0 \quad (15)$$

3. Solution

When a small-amplitude deflection for the pipe is under consideration, the deformation is infinitesimal. In this condition, the constitutive relations are linear, and the linear vibrational analysis for the system is reliable. On the other hand, when the pipe is subjected to high transverse loads and a large deflection is considered for the system, the mid-plane stretching effect due to immovable boundary conditions is crucial and should be considered in the model. In this situation, the problem is nonlinear, and nonlinear vibrational analysis of the system is of great importance (Taati et al., 2020; Tang and Yang, 2018). Therefore, both linear and nonlinear vibration analyses are essential for the system under the actual operating conditions. In this section, the procedure to obtain linear and nonlinear vibrational frequencies of the system is explained.

3.1. Linear vibrational analysis

3.1.1. Two-phase flow

To acquire the reduced-order model of the considered system, the partial differential equation of the system is transformed into ordinary differential equations utilizing the Galerkin discretization approach. Based on this method, spatial and temporal components of the model equation become separated from each other. In this technique, the transverse deflection of the system is expanded as a series of basic

functions (Roodgar Saffari et al., 2020a):

$$y(x, t) = \sum_{j=1}^n \varphi_j(x) q_j(t) \quad (16)$$

in which $q(t)$ is the time-dependent generalized coordinate and n is the number of considered vibrational modes for the system. Also, $\varphi(x)$ is the approximate mode shape function (eigenfunction) for the related end conditions of the system. For the P-P, C-C, and C-F boundary conditions, relevant eigenfunctions are given, respectively, as follows (Ebrahimi-Mamaghani et al., 2020; Roodgar Saffari et al., 2020b):

$$\varphi_j(x) = \sin\left(j\pi\frac{x}{L}\right) \quad (17)$$

$$\varphi_j(x) = \cosh\left(\lambda_j\frac{x}{L}\right) - \cos\left(\lambda_j\frac{x}{L}\right) - \frac{\sin(\lambda_j) + \sin(\lambda_j)}{\cos(\lambda_j) + \cosh(\lambda_j)} \left(\sinh\left(\lambda_j\frac{x}{L}\right) - \sin\left(\lambda_j\frac{x}{L}\right) \right) \quad (18)$$

$$\varphi_j(x) = \cosh\left(\lambda_j\frac{x}{L}\right) - \cos\left(\lambda_j\frac{x}{L}\right) - \frac{\sin(\lambda_j) - \sin(\lambda_j)}{\cos(\lambda_j) + \cosh(\lambda_j)} \left(\sinh\left(\lambda_j\frac{x}{L}\right) - \sin\left(\lambda_j\frac{x}{L}\right) \right) \quad (19)$$

It is essential to note that values of λ_j in Eqs. (18) and (19) can be computed numerically from the characteristic relations $\cosh(\lambda_j)\cos(\lambda_j) - 1 = 0$ and $\cosh(\lambda_j)\cos(\lambda_j) + 1 = 0$, respectively (Sun et al., 2021). The first eight values of λ_j are illustrated in Table 1.

The nonlinear term is ignored for linear vibrational analysis of the system, and the orthogonality property of shape modes is used (Ebrahimi-Mamaghani et al., 2016). Inserting Eq. (16) into the linear dynamical equation of the system, multiplying the resultant by $\varphi_j(x)$, and then integrating over the whole length of the pipe, one can obtain n differential equations which can be rewritten in the matrix form as follows:

$$\mathbf{M}\ddot{\mathbf{q}}(t) + \mathbf{C}\dot{\mathbf{q}}(t) + \mathbf{K}\mathbf{q}(t) = 0 \quad (20)$$

where the dot indicates the derivative with respect to time.

Eq. (20) is the discretized dynamical equation of the system in the matrix form. In this equation, \mathbf{K} is the stiffness matrix, \mathbf{M} is the mass matrix, and \mathbf{C} is the damping matrix. Also, \mathbf{q} is the time-dependent vector of generalized coordinates of the system. These matrices are defined as:

$$\mathbf{q} = [q_1(t), q_2(t), \dots, q_n(t)]^T \quad (21)$$

$$\mathbf{M}_{sr} = (\rho_p A_p + \rho_L (1 - \alpha_G) A_C + \rho_G \alpha_G A_C) \int_0^L \varphi_s(x) \varphi_r(x) dx \quad (22)$$

Table 1
Values of λ_j in Eqs. (18) and (19).

<i>J</i>	Boundary condition	
	C-C	C-F
1	4.73	1.87
2	7.85	4.69
3	10.99	7.85
4	14.13	10.99
5	17.27	14.13
6	20.42	17.27
7	23.56	20.42
8	26.7	23.56

$$\mathbf{C}_{sr} = EI \frac{\sigma}{\Omega} \int_0^L \varphi_s(x) \frac{\partial^4 \varphi_r(x)}{\partial x^4} dx + 2 \left(\rho_L (1 - \alpha_G) A_C \left(V - \frac{\alpha_G U_{GM}}{1 - \alpha_G} \right) \right. \\ \left. + \rho_G \alpha_G A_C (U_{GM} + V) \right) \int_0^L \varphi_s(x) \frac{\partial \varphi_r(x)}{\partial x} dx + c \int_0^L \varphi_s(x) \varphi_r(x) dx \quad (23)$$

$$\mathbf{K}_{sr} = EI \int_0^L \varphi_s(x) \frac{\partial^4 \varphi_r(x)}{\partial x^4} dx + \left(\rho_L (1 - \alpha_G) A_C \left(V - \frac{\alpha_G U_{GM}}{1 - \alpha_G} \right)^2 \right. \\ \left. + \rho_G \alpha_G A_C (U_{GM} + V)^2 - T \right) \int_0^L \varphi_s(x) \frac{\partial^2 \varphi_r(x)}{\partial x^2} dx \pm (\rho_P A_P + \rho_L (1 - \alpha_G) A_C \\ + \rho_G \alpha_G A_C) g \int_0^L \varphi_s(x) \left((x - L) \frac{\partial^2 \varphi_r(x)}{\partial x^2} + \frac{\partial \varphi_r(x)}{\partial x} \right) dx \quad (24)$$

The second-order matrix form of Eq. (20) can be degenerated to the first-order one by the following procedure (Paidoussis, 1998; Bahaadini et al., 2018):

$$\mathbf{B} \dot{\mathbf{Z}}(t) + \mathbf{E} \mathbf{Z}(t) = 0 \quad (25)$$

in which

$$\mathbf{B} = \begin{bmatrix} 0 & \mathbf{M} \\ \mathbf{M} & \mathbf{C} \end{bmatrix}, \quad \mathbf{E} = \begin{bmatrix} -\mathbf{M} & 0 \\ 0 & \mathbf{K} \end{bmatrix}, \quad \mathbf{Z}(t) = \begin{bmatrix} \dot{\mathbf{q}}(t) \\ \mathbf{q}(t) \end{bmatrix} \quad (26)$$

Assuming the exponential form $\mathbf{Z}(t) = \mathbf{P} e^{i\omega_L t}$ for the solution of Eq. (25) results in the following eigenvalue problem:

$$\mathbf{Y} \mathbf{P} - i\omega_L \mathbf{I} = 0 \quad (27)$$

where $\mathbf{Y} = -\mathbf{B}^{-1}\mathbf{E}$, \mathbf{I} is the identity matrix, and ω_L is the linear circular frequency of motion that can be computed in terms of key parameters, such as gas void fraction, flow mixture velocity, geometrical and physical properties of the system.

3.1.2. Single-phase flow

The linear dynamical equation for the single-phase system by considering gravitational and damping effects can be expressed as (Monette and Pettigrew, 2004):

$$EI \left(1 + \frac{\sigma}{\Omega} \frac{\partial}{\partial t} \right) \frac{\partial^4 y}{\partial x^4} \pm (\rho_P A_P + \rho_L A_C) g \left((x - L) \frac{\partial^2 y}{\partial x^2} + \frac{\partial y}{\partial x} \right) + (\rho_L A_C U_L^2 - T) \frac{\partial^2 y}{\partial x^2} \\ + 2\rho_L A_C U_L \frac{\partial^2 y}{\partial x \partial t} + c \frac{\partial y}{\partial t} + (\rho_P A_P + \rho_L A_C) \frac{\partial^2 y}{\partial t^2} = 0 \quad (28)$$

To generalize the model equation, the following dimensionless parameters are introduced:

$$\xi = \frac{x}{L}, \quad \eta = \frac{y}{L}, \quad \tau = \frac{t}{L^2} \sqrt{\frac{EI}{\rho_P A_P + \rho_L A_C}}, \quad \beta = \frac{\rho_L A_C}{\rho_P A_P + \rho_L A_C}, \\ u_L = U_L L \left(\frac{\rho_L A_C}{EI} \right)^{0.5}, \quad \gamma = g L^3 \frac{\rho_P A_P + \rho_L A_C}{EI}, \quad P = \frac{TL^2}{EI} \\ \xi_s = \frac{\sigma}{\Omega L^2} \sqrt{\frac{EI}{\rho_P A_P + \rho_L A_C}}, \quad \xi_{2\varphi} = \frac{CL^2}{\sqrt{EI(\rho_P A_P + \rho_L A_C)}} \quad (29)$$

Substituting the dimensionless parameters in Eq. (28) yields the following non-dimensional governing dynamical equation:

$$\left(1 + \xi_s \frac{\partial}{\partial \tau} \right) \frac{\partial^4 \eta}{\partial \xi^4} \pm \gamma \left((\xi - 1) \frac{\partial^2 \eta}{\partial \xi^2} + \frac{\partial \eta}{\partial \xi} \right) + (u_L^2 - P) \frac{\partial^2 \eta}{\partial \xi^2} + 2\sqrt{\beta_L} u_L \frac{\partial^2 \eta}{\partial \xi \partial \tau} \\ + \xi_{2\varphi} \frac{\partial \eta}{\partial \tau} + \frac{\partial^2 \eta}{\partial \tau^2} = 0 \quad (30)$$

Dimensionless linear circular frequencies ($\bar{\omega}_L = \omega_L L^2 \left(\frac{\rho_P A_P + \rho_L A_C}{EI} \right)^{0.5}$) can be obtained by solving the eigenvalue problem of Eq. (30)

3.1.3. Damping sources

Comprehensive and efficient simulation of industrial piping systems is not acceptable without any reference to the damping effects. Besides, since damping in the two-phase flow is much higher than in the single-phase, considering the damping effects in the mathematical models of pipes conveying two-phase flow is decisive. The damping sources of systems transporting two-phase flow can be classified as follows: structural damping, viscous damping, flow-dependent damping, and the two-phase component of damping (Charreton et al., 2015). In an experimental effort, Carlucci (1980) examined the hydrodynamics of pipes conveying two-phase flow. He found that the contributions of viscous and flow damping effects are negligible compared to structural and two-phase damping effects. As a result, the resultant damping ratio (ξ_{tot}) in the system can be considered as the sum of the structural damping (ξ_s) and the two-phase component of damping ($\xi_{2\varphi}$) as follows (Li et al., 2020):

$$\xi_{tot} \approx \xi_s + \xi_{2\varphi} \quad (31)$$

Gravelle et al. (2007) analyzed the vibrational characteristics of brass and PVC pipes with various two-phase flow parameters and different flow regimes. They detected the two-phase damping behavior of the system in terms of gas void fraction and flow mixture velocity. In Fig. 2, the flow pattern map for vertical pipes is shown (Taitel et al., 1980), and the most generally recognized regimes are depicted. The markers on the indicated curves are related to gas void fractions valued 0.1, 0.2, ..., 0.9. Also, the extracted experimental data from Ref (Gravelle et al., 2007) for the two-phase damping ratio of PVC pipe against the gas void fraction are depicted in Fig. 3. Gravelle et al. (2007) reported that the two-phase damping ratio of the system reaches its maximum value near the transition zone. (Taitel et al., 1980), (Gravelle et al., 2007)

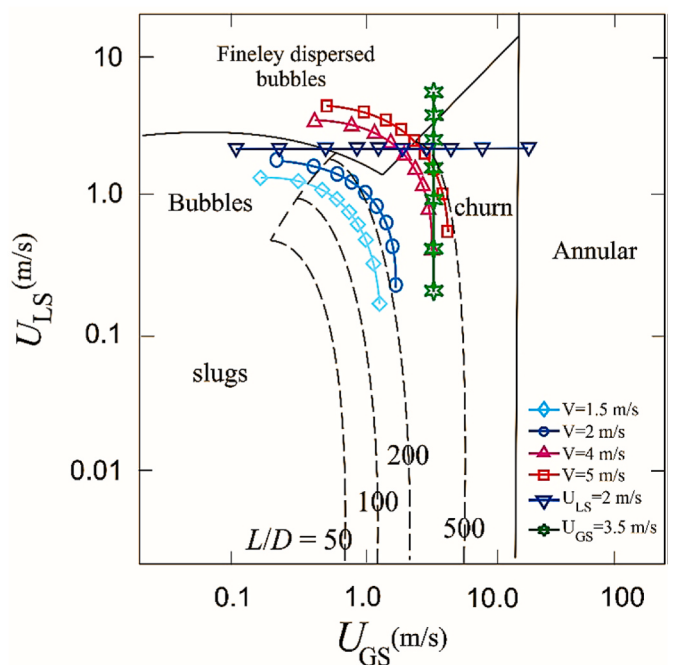


Fig. 2. Flow pattern map of vertical pipes conveying air-water two-phase (25 °C, $D_i = 2.5$ cm, and 10 N/cm²).

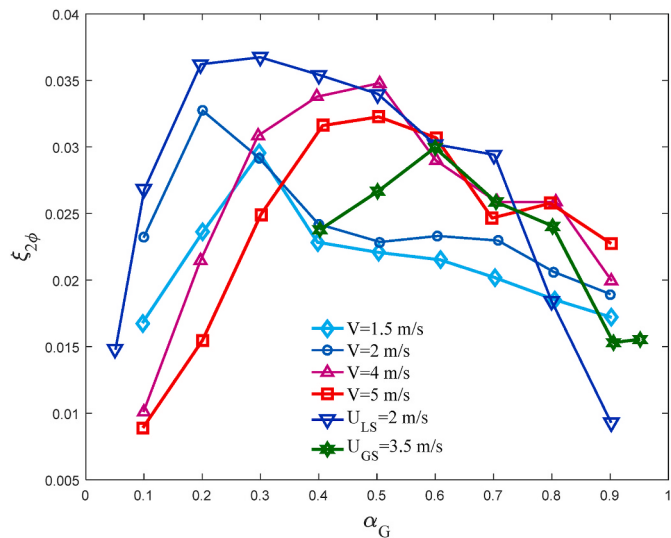


Fig. 3. Two-phase damping ratio of the PVC pipe versus the gas void fraction.

3.2. Nonlinear vibrational analysis

To acquire the closed-form expression for the nonlinear vibrational frequency of the system, the Galerkin approach utilizing one approximate vibrational mode was considered:

$$y(x, t) = \varphi_1(x)q_1(t) \quad (32)$$

By eliminating the damping effects and applying the single-mode Galerkin method, the following equation is obtained:

$$\theta \frac{d^2 q_1(t)}{dt^2} + \chi_1 q_1(t) + \chi_3 q_1^3(t) = 0 \quad (33)$$

in which the coefficients of Eq. (33) are explicitly expressed as follows:

$$\theta = (\rho_p A_p + \rho_L(1 - \alpha_G)A_C + \rho_G \alpha_G A_C) \int_0^L \varphi_1^2(x) dx \quad (34)$$

$$\begin{aligned} \chi_1 &= EI \int_0^L \varphi_1(x) \frac{\partial^4 \varphi_1(x)}{\partial x^4} dx + \left(\rho_L(1 - \alpha_G)A_C \left(V - \frac{\alpha_G U_{GM}}{1 - \alpha_G} \right)^2 \right. \\ &\quad \left. + \rho_G \alpha_G A_C (U_{GM} + V)^2 - T \right) \int_0^L \varphi_1(x) \frac{\partial^2 \varphi_1(x)}{\partial x^2} dx \pm (\rho_p A_p + \rho_L(1 - \alpha_G)A_C \\ &\quad + \rho_G \alpha_G A_C) g \int_0^L \varphi_1(x) \left((x - L) \frac{\partial^2 \varphi_1(x)}{\partial x^2} + \frac{\partial \varphi_1(x)}{\partial x} \right) dx \end{aligned} \quad (35)$$

$$\chi_3 = -\frac{EA_p}{2L} \int_0^L \left(\frac{\partial \varphi_1(x)}{\partial x} \right)^2 dx \int_0^L \varphi_1(x) \frac{\partial^2 \varphi_1(x)}{\partial x^2} dx \quad (36)$$

Eq. (33) is a Duffing-like nonlinear differential equation. It is numerically proved that depending on the value of χ_3 , weakly and strongly nonlinear cases are probable. Therefore, using traditional perturbation methods such as harmonic balance and multiple scales is not always valid. To obtain the exact dynamical response of the system, one can implement the first-order approximation of the homotopy analysis method (Jamshidifar et al., 2018; Zhang and Ali, 2021), which has high efficiency in both strongly and weakly nonlinear equations. For the strongly nonlinear vibration of beam-like structures, Pirbodaghi et al. (2009) acquired the following analytical solution for the free vibrational response:

$$q(t) \approx \frac{A}{32\omega_{NL}^2} \left(\frac{\chi_3}{\theta} A^2 + 32\omega_{NL}^2 \right) \cos(\omega_{NL}t) - \frac{\chi_3}{32\theta\omega_{NL}^2} A^3 \cos(3\omega_{NL}t) \quad (37)$$

where A is the initial vibrational amplitude of the system. Also, ω_{NL} is the nonlinear circular frequency of motion and can be written as:

$$\omega_{NL} = \sqrt{\frac{3\chi_3 A^2 + 4\chi_1}{4\theta}} \quad (38)$$

According to Eq. (38), contrary to the linear circular frequency, the instant nonlinear circular frequency of the system has a strong dependency on the initial vibrational amplitude.

4. Results and discussion

In this section, first, the results of the present model are compared and validated with those published in the literature. Then, the impact of

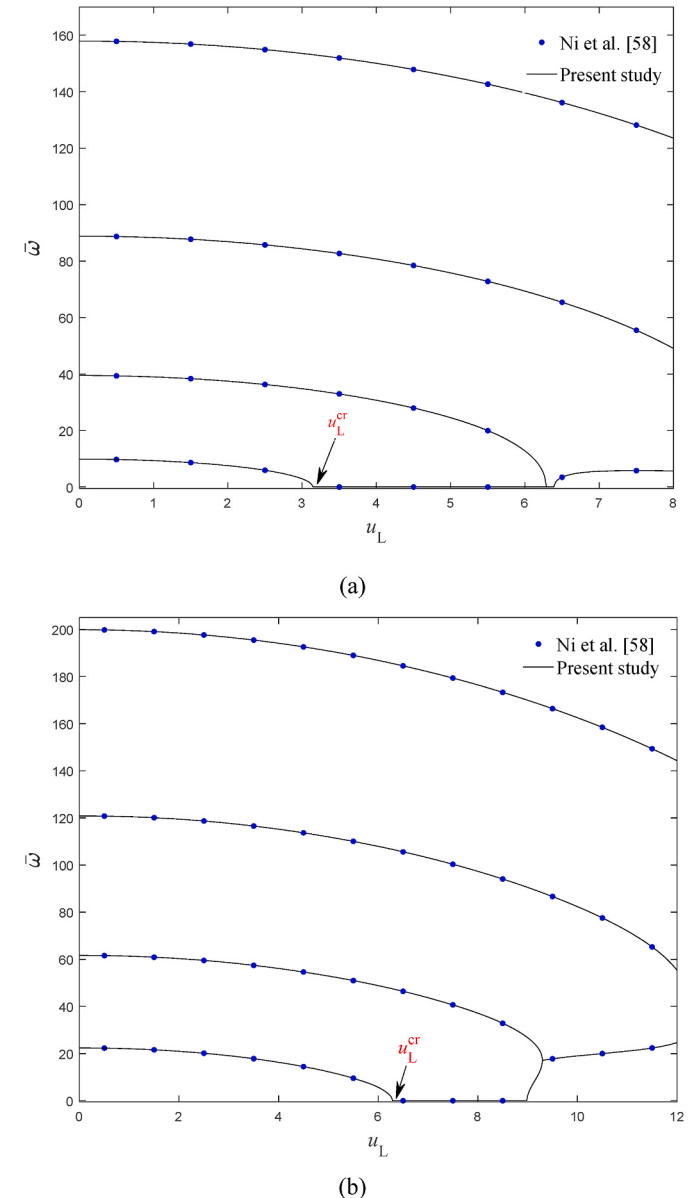


Fig. 4. Dimensionless linear vibrational frequencies of pipes conveying single-phase flow versus the dimensionless fluid velocity for (a) simply supported and (b) doubly clamped boundary conditions in the absence of the tension force, gravitational and damping effects.

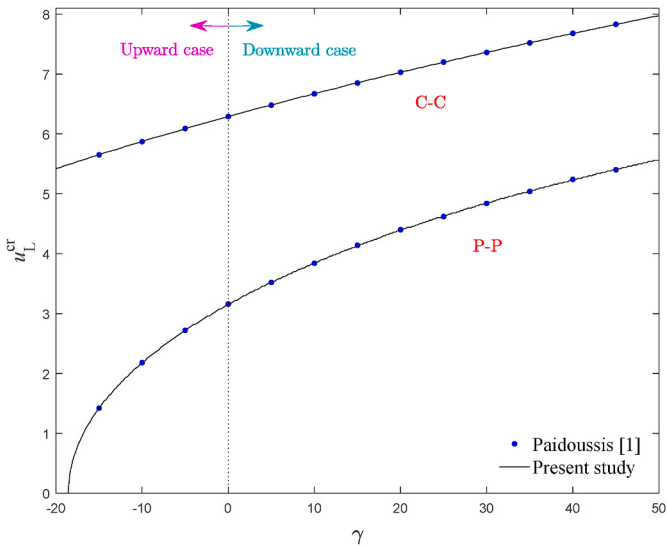


Fig. 5. Dimensionless critical fluid velocity of supported pipes conveying single-phase flow versus the gravity parameter in the absence of the tension force and damping effects.

various parameters on the linear and nonlinear vibrational frequencies is investigated.

4.1. Comparison study

For the verification, dimensionless natural vibrational frequencies of supported pipes conveying single-phase flow against the dimensionless fluid velocity are demonstrated in Fig. 4 (a, b). It can be seen in these figures, the acquired outcomes of the current study have an appropriate consistency with those reported by Ni et al. (2011) based on the differential transformation method. As demonstrated in these figures, when the fundamental vibrational frequency of the pipe reaches zero, the system undergoes static instability (buckling). Hence, the fundamental vibrational frequency analysis is crucial for vibration controlling of piping structures. Also, it should be pointed out that the fluid velocity in which the system experiences the buckling phenomenon is regarded as the critical fluid velocity (u_{cr}).

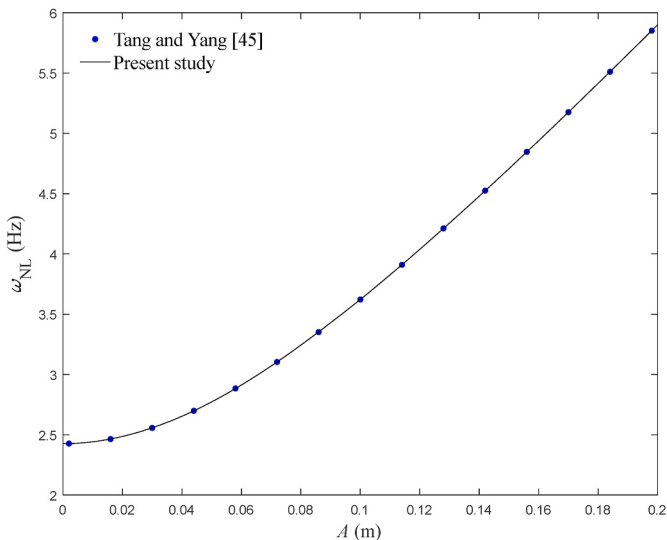


Fig. 6. Nonlinear vibrational frequency of the simply supported pipe conveying single-phase flow versus the initial vibrational amplitude in the absence of gravitational and damping effects.

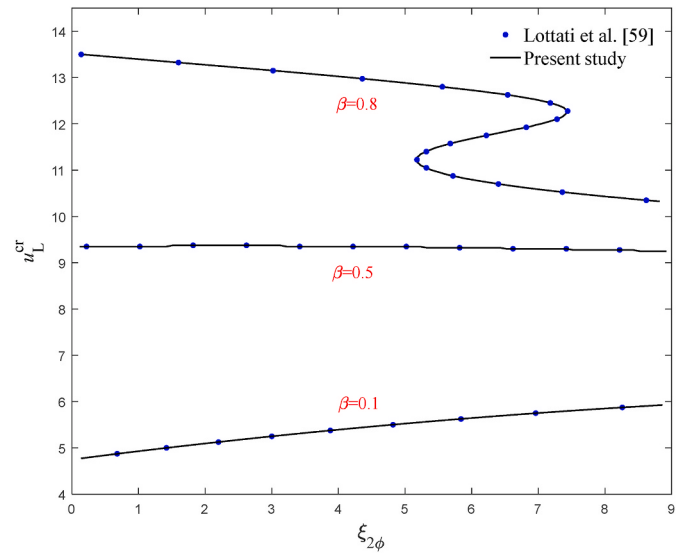


Fig. 7. Dimensionless critical fluid velocity of clamped-free pipes conveying single-phase flow versus the dimensionless internal damping in the absence of tension force and gravitational effects.

In Fig. 5, the dimensionless critical fluid velocity of supported pipes transporting single-phase flow against the gravity parameter, γ , is plotted. It is observed in this figure that the numerical results of the current investigation are in accordance with the analytical outcomes of Paidoussis (1998). It should be stated that positive (negative) gravitational parameters are related to downward (upward) pipes.

The nonlinear vibrational frequency of a simply supported pipe conveying single-phase flow against the initial vibrational amplitude is depicted in Fig. 6. It is obvious that the obtained results are in satisfactory agreement with those reported by Tang and Yang (2018). The geometrical and physical properties of the considered system are $U_L = 100$ m/s, $L = 10$ m, $E = 70$ Gpa, $\rho_L = 1000$ kg/m³, $T = -20$ N/m, inner diameter = 0.08 m, and outer diameter = 0.1 m.

For more validation, the stability diagram of horizontal clamped-free pipes conveying single-phase flow is depicted in Fig. 7. This figure shows the dimensionless critical fluid velocity of cantilevered pipes

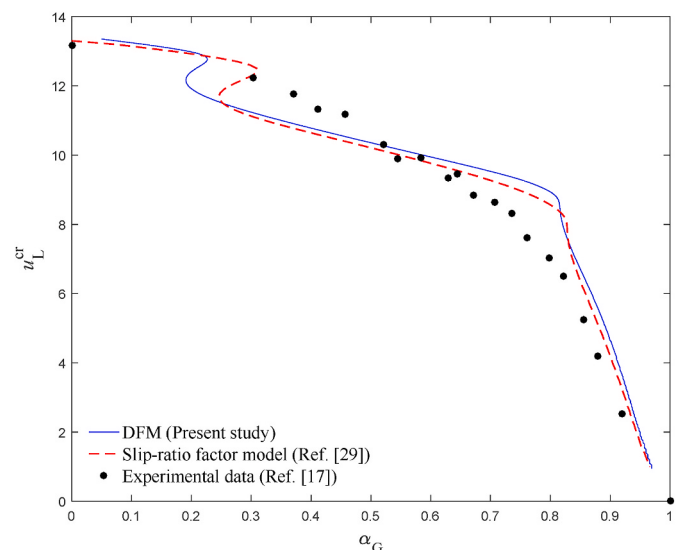


Fig. 8. Comparison between theoretical and experimental data of dimensionless critical liquid-phase velocity of a downward cantilevered pipe carrying two-phase flow versus the gas void fraction for conditions of Table 2 in the absence of the tension force.

Table 2

Properties of the experimental setup used by Monette and Pettigrew (2004)

EI (N.m ²)	L (m)	m_p (kg/m ³)	D_i (m)	Σ	$\xi_{2\phi}$
0.003	0.547	65.7×10^{-3}	9.25×10^{-3}	0.1	0.12

Table 3

Physical and geometrical properties of the test section used by Gravelle et al. (2007)

Property	Material	
	Brass	PVC
Length, L (m)	1.45	1.48
Inner diameter, D_i (mm)	18	21.2
Outer diameter, D_o (mm)	19	26.6
Young modulus, E (GPa)	100	2.4
Mass per unit length, m_p (kg/m)	0.254	0.309
Structural damping ratio, ξ_s (%)	0.07	0.7

transporting single-phase flow against the dimensionless internal damping for different fluid mass ratios, β . It is clear that the obtained results of the current study are in excellent agreement with those reported by Lottati et al. (Lottati and Kornecki, 1986).

Fig. 8 depicts the dimensionless critical liquid-phase velocity of a downward cantilevered pipe conveying two-phase flow as a function of the gas void fraction for the conditions of Table 2. This figure compares the calculated critical liquid-phase velocity of the considered system based on the DFM and the slip-ratio factor model (Ebrahimi-Mamaghani et al., 2019) with the experimental data reported by Monette and Pettigrew (2004). According to this figure, an acceptable agreement is observed between the theoretical results and those reported experimentally. Also, the difference between the presented results is more obvious for the moderate values of the gas void fraction.

4.2. Parametric study

In the following, to obtain the numerical results of the present investigation, the geometrical and physical properties of the experimental setup used by Gravelle et al. (2007), which are listed in Table 3, were considered. It should be mentioned that in the following of the present study, the effect of the initial axial tension force is ignored.

In Table 4, the first linear circular frequency of the doubly clamped PVC pipe in terms of the gas void fraction is tabulated for $V = 4$ m/s, and gravitational and damping effects on the system vibration are perused. It is evident that at a constant flow mixture velocity condition, the linear circular frequency enhances as the gas void fraction increases. The reason for this trend is that when the gas phase contribution rises in the pipe by increasing the gas void fraction, the effective mass and internal flow forces decrease; thus, the circular frequency increases. Based on Table 4, considering hysteresis and two-phase damping effects for pipes leads to the decrease of the linear circular frequency. Because the two-phase damping reaches its maximum value at the flow transition

Table 5

First linear circular frequency (rad/s) of the upward doubly clamped PVC pipe tube by considering damping effects.

α_G	$V = 1.5$ m/s	$V = 2$ m/s	$V = 4$ m/s	$V = 5$ m/s
0.1	76.192	76.1506	75.623	75.445
0.2	78.452	78.413	77.905	77.754
0.3	80.922	80.887	80.399	80.277
0.4	83.638	83.608	83.140	83.048
0.5	86.644	86.618	86.171	86.111
0.6	89.996	89.974	89.549	89.522
0.7	93.765	93.748	93.344	93.353
0.8	98.046	98.034	97.652	97.700
0.9	102.967	102.960	102.600	102.690

point, one can conclude that the damping effects have the most decreasing effect on the linear circular frequency around the flow transition region. Undoubtedly, the impact of the structural damping compared to the two-phase damping effect is more sensible. This feature can be justified by comparing structural and two-phase damping coefficients in the damping matrix (Eq. (23)). Also, compared with the upward-oriented flow case, the pipe conveying downward flow has a greater circular frequency. Paidoussis (1998) indicated that gravitational force has a decreasing/increasing effect on the effective stiffness of upward/downward pipes containing single-phase flow. In other words, when the flow is upward (downward), the gravity force is in the opposite (same) direction of the flow orientation. In such conditions, the applied gravitational force is compressive (tensile) load, and the circular frequency and instability resistance of the system weakens (strengthens). As a result, due to the stiffness-hardening effect of gravitational force, the linear circular frequency of pipes conveying downward two-phase flow is higher than in the upward case. This condition is previously reported in the literature for the single-phase case (see Fig. 5).

In Table 5, the first linear circular frequency of upward doubly clamped PVC pipes involving damping effects is illustrated for various gas void fractions and flow mixture velocities. As expected, for all values of the flow mixture velocity, the linear circular frequency of the system increases with increasing the gas void fraction. On the other hand, when the gas void fraction is constant, the linear circular frequency descends with ascending flow mixture velocity. The reason for the occurrence of this phenomenon is that due to the destabilizing effects of the centrifugal force of internal flow, the effective stiffness of the system decreases by increasing the flow velocity. Similar to this phenomenon also occurs in the single-phase case (see Fig. 4).

Generally, when the system operates in the churn, bubble, or finely dispersed bubble flow conditions, the circular frequency reduces by ascending the flow mixture velocity at a constant gas void fraction. The reason for this behavior is the increment of the centrifugal force, and consequently, the decrement of the effective stiffness of the system by increasing the flow mixture velocity. For $V = 1.5$ and 2 m/s, by increasing the gas void fraction, the flow regime of the system changes from the finely dispersed bubble to the churn. In such a situation, the

Table 4First linear circular frequency (rad/s) for a doubly clamped PVC pipe for $V = 4$ m/s.

α_G	Upward-oriented flow			Downward-oriented flow		
	Ignoring damping effects	with structural damping	with two-phase damping	Ignoring damping effects	with structural damping	with two-phase damping
0.1	75.862	75.625	75.861	76.403	76.168	76.402
0.2	78.151	77.907	78.150	78.683	78.440	78.680
0.3	80.652	80.401	80.651	81.173	80.924	81.172
0.4	83.401	83.142	83.400	83.910	83.653	83.908
0.5	86.441	86.173	86.440	86.937	86.670	86.934
0.6	89.829	89.551	89.828	90.310	90.032	90.309
0.7	93.636	93.346	93.635	94.098	93.810	94.097
0.8	97.956	97.654	97.955	98.398	98.097	98.397
0.9	102.920	102.602	102.919	103.336	103.020	103.334

Table 6

First linear circular frequency of upward doubly clamped PVC tube by considering damping effects.

$U_{LS} = 2 \text{ m/s}$		$U_{GS} = 3.5 \text{ m/s}$	
α_G	$\omega_L \text{ (rad/s)}$	α_G	$\omega_L \text{ (rad/s)}$
0.05	75.080	0.4	83.935
0.1	76.130	0.5	86.025
0.2	78.367	0.6	89.463
0.3	80.811	0.7	93.320
0.4	83.493	0.8	97.687
0.5	89.738	0.9	102.682
0.6	93.400	0.95	105.632
0.7	95.473		
0.8	98.128		
0.9	101.787		

circular frequency increases due to reducing the effective mass of the system and internal flow forces. It should be noted that when $\alpha_G \approx 0.25$, due to the two-phase damping effect near the transition zone, the increment of the circular frequency of the system by the ascent of the gas void fraction decreases to some extent. On the other hand, for $V = 4$ and 5 m/s , by decreasing the gas void fraction in the system, the flow regime changes from the churn to the bubble, and the circular frequency decreases. This decrement is more noticeable around the transition region, i.e., $\alpha_G \approx 0.5$ (see Table 5 and Fig. 3).

In Table 6, the linear circular frequency of the doubly clamped system is given for $U_{LS} = 2 \text{ m/s}$ and $U_{GS} = 3.5 \text{ m/s}$. This Table demonstrates that by increasing α_G , the linear circular frequency increases. When $U_{GS} = 3.5 \text{ m/s}$, as the superficial liquid velocity ascends in the system, the flow regime first changes from bubble to finely dispersed bubble, and then the system operates under the churn flow regime. This flow regime evolution changes the circular frequency of the system. During this flow regime change, the flow mixture velocity and the gas void fraction increase. In this condition, compared with the decreasing effect of the flow mixture velocity, the increasing effect of the gas void fraction on the circular frequency of the system is dominant. So that the circular frequency of the system overall increases by this regime change. When $U_{LS} = 2 \text{ m/s}$, as the superficial gas velocity ascends, the gas void fraction decreases while the flow mixture velocity increases. In this case, the flow regime changes from the churn to the finely dispersed bubble. As a result, the circular frequency of the system declines. Also, in this condition, the circular frequency decreases more in comparison with the case of constant flow mixture velocity. Also, based on the

aforementioned results and by comparing Tables 4–6, it can be concluded, one can deduce that the system has the highest and lowest circular frequency for churn and finely dispersed bubbly flow regimes, respectively.

Ebrahimi-Mamaghani et al. (2019) demonstrated that in the case of clamped-free boundary conditions (nonconservative systems), pipes conveying two-phase flow, compared with pipes conveying single-phase flow, have a lower frequency. While for pipes with restrained boundary conditions, this trend is reversed. In other words, in the case of supported boundary conditions (conservative systems), pipes conveying two-phase flow have a higher frequency than single-phase cases. In general, from the point of view of adjusting the dynamical behavior, pipes conveying two-phase flow are more flexible than pipes conveying single-phase flow.

In the following, the vibration of PVC pipes with P-P boundary conditions is investigated by considering damping and gravitation effects, unless otherwise is expressed. In Fig. 9, linear and nonlinear vibrational frequencies against flow mixture velocity are illustrated for different gas void fractions. It can be observed in this figure that by increasing the flow mixture velocity/gas void fraction in the system, both linear and nonlinear vibrational frequencies decrease/increase. Vibrational frequencies have a higher sensitivity to the variation of gas void fraction and slightly vary with the flow mixture velocity variation. Also, the nonlinear vibrational frequency curves are above the linear vibrational frequency curves. Besides, since gas void fraction and flow mixture velocity have opposite effects on vibrational frequencies, one can introduce these parameters as vibrational control factors in the piping systems from the design point of view.

Linear and nonlinear vibrational frequencies against the outer diameter of the pipe with different initial vibrational amplitudes and gas void fractions are depicted in Fig. 10 for $V = 4 \text{ m/s}$. The flexural rigidity (EI) of the system increases by increasing the outer cross-sectional area of the pipe. Therefore, both linear and nonlinear vibrational frequencies ascend by an increase in the outer diameter. Also, it can be observed that the vibrational frequency increases by increasing the gas void fraction, especially at a high outer diameter of the pipe. In Eq. (38), when the initial vibrational amplitude of the system becomes zero, the nonlinear vibrational frequency is reduced to the linear one. As a result, the nonlinear vibrational frequency is higher than that of the linear. Besides, the more the initial vibrational amplitude, the more the linear vibrational frequency becomes.

Variations of linear and nonlinear vibrational frequencies against the inner diameter of pipe are shown in Fig. 11 (a, b), respectively, for

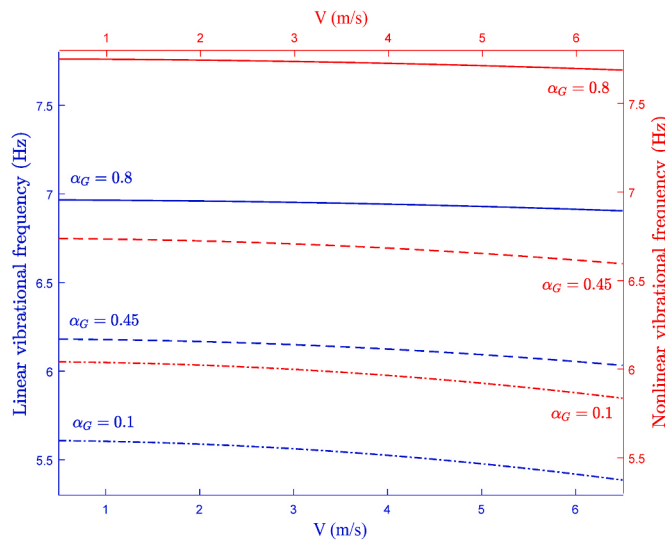


Fig. 9. Vibrational frequencies of the system versus the flow mixture velocity for $A = 0.01 \text{ m}$.

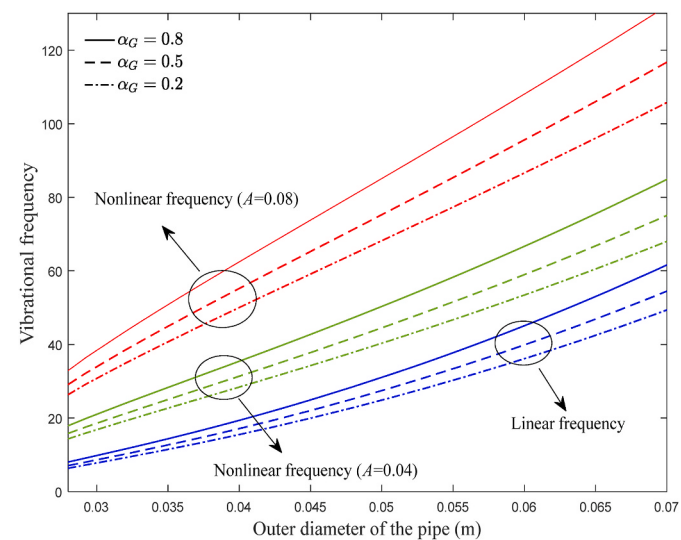
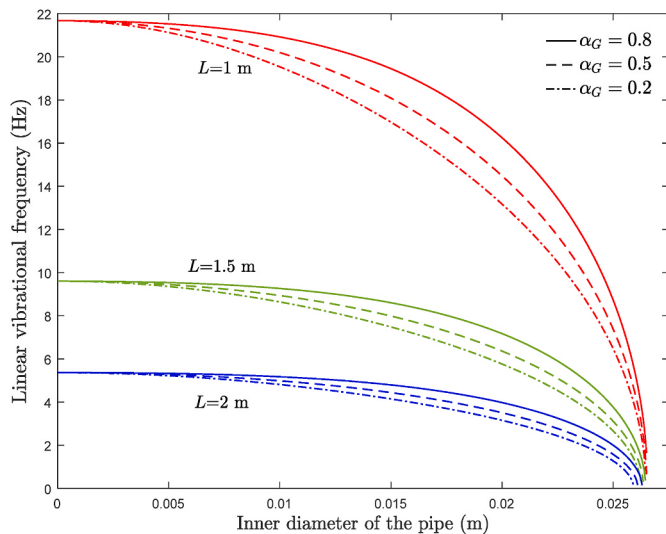
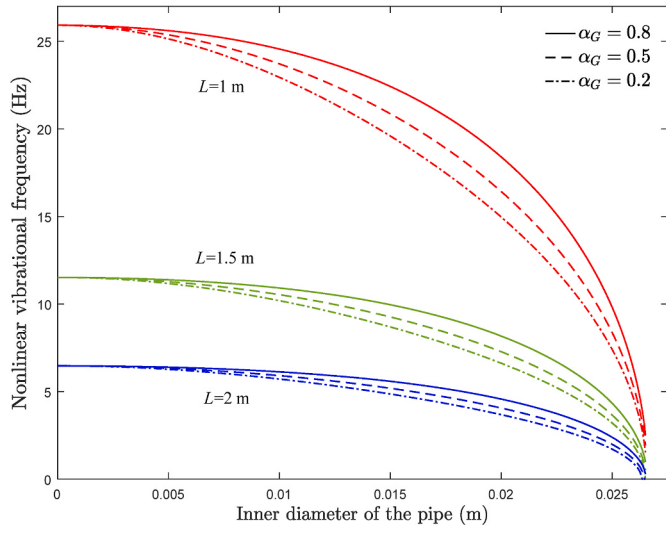


Fig. 10. Vibrational frequencies of the system versus the outer diameter for $V = 4 \text{ m/s}$.



(a)

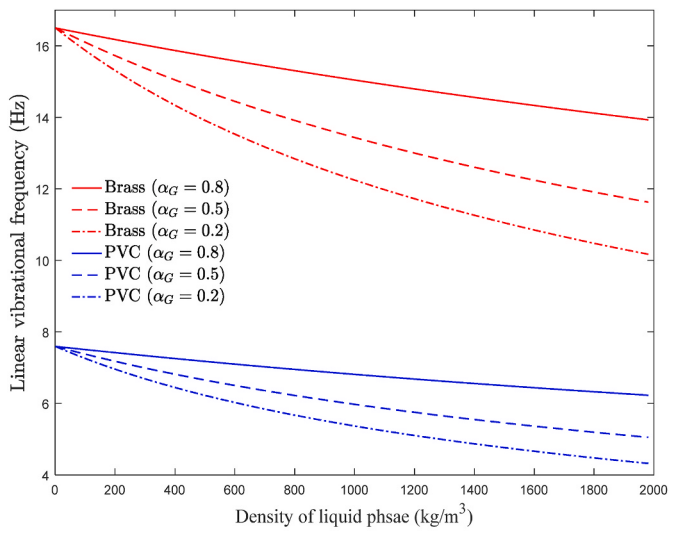


(b)

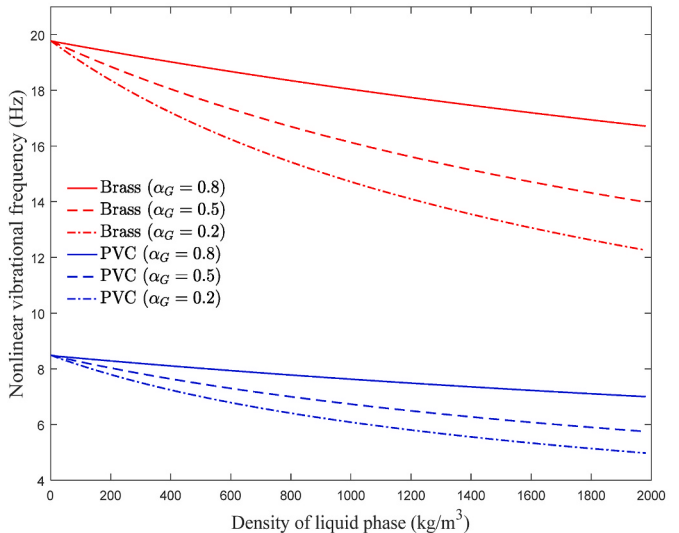
Fig. 11. (a) Linear and (b) nonlinear vibrational frequencies of the system versus the inner diameter for $V = 4 \text{ m/s}$ and $A = 0.01 \text{ m}$.

various gas void fractions and pipe lengths. For relatively small values of D_i , an increase in the inner diameter has a slight decreasing impact on the vibrational frequencies. While when the inner diameter approaches the outer diameter, a rapid decrement in vibrational frequencies can be observed by an increase in the inner diameter. It is worth noting that at high values of the inner diameter, vibrational frequencies converge to zero, and the system loses its stability. As a result, it can be mentioned that high values of the inner diameter have a notable impact on the system dynamics. In fact, it is generally known that when the pipe length ascends, the system becomes more slender. In this condition, the effective stiffness of the system decreases for longer pipes. Therefore, decreasing the pipe length yields to the enhancement of vibrational frequencies. Also, rising the gas void fraction in the system yields the increment of vibrational frequencies, especially for moderate values of inner diameter. Moreover, the nonlinear frequency is higher than the linear.

The evolution of linear and nonlinear vibrational frequencies against the liquid density is exhibited in Fig. 12 (a) and (b), respectively. The effect of pipe material and gas void fraction on the vibrational behavior



(a)



(b)

Fig. 12. (a) Linear and (b) nonlinear vibrational frequencies of the system versus the liquid-phase density for $V = 4 \text{ m/s}$ and $A = 0.01 \text{ m}$.

of the system is also shown in these figures. By increasing the liquid density in the piping systems, the mass flux of internal flow ascends. Hence, the vibrational frequency decreases by increasing the liquid density. One can expect that at high liquid density, the frequency vanishes, and the system experiences static instability. A noteworthy issue in these figures is the effect of pipe material on vibrational frequencies. The variation trends are similar for both types of pipes. Since the flexural rigidity and mass per unit length of brass pipe compared with those of PVC pipe are higher and lower, respectively, one can conclude that the vibrational frequencies of the brass pipes are higher. Hence, one can expect that the instability threshold of the brass pipes is higher. In general, the appropriate selection of physical and geometrical characteristics of piping systems conveying two-phase flow plays an important role in the dynamical behavior and vibrational stability of the system. In addition, as expected, for all values of the liquid density, the nonlinear frequency is higher than the linear, especially for the brass pipe. As a result, the liquid density provides an excessive degree of freedom to tune the vibrational frequencies of systems conveying two-phase flow. Also, vibrational frequencies increase by increasing the gas void fraction,

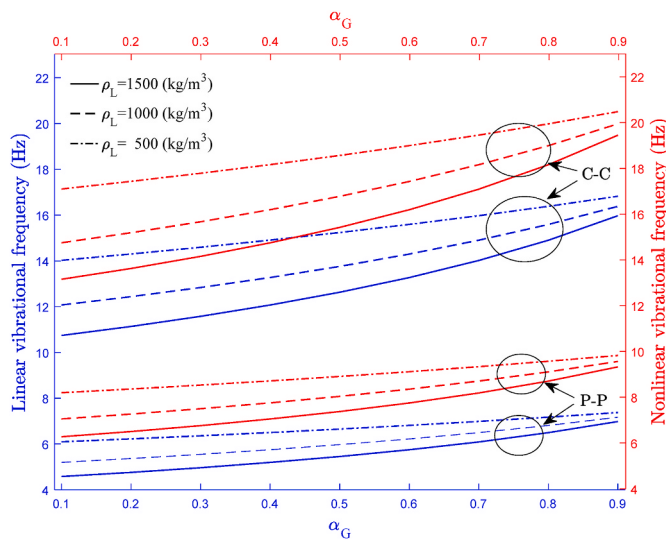


Fig. 13. Vibrational frequencies of the system versus the gas void fraction for $V = 4 \text{ m/s}$ and $A = 0.0175 \text{ m/s}$.

especially for denser flows.

In Fig. 13, the dependence of vibrational frequencies on the gas void fraction is examined. The role of boundary conditions and liquid density in the vibrational behavior of the system is also investigated. Based on this figure, linear and nonlinear vibrational frequencies increase by increasing gas void fraction and liquid density. Also, at high values of gas void fraction, the variation of liquid density has a lower impact on the vibrational behavior of the system. This feature can be explained by the fact that by increasing the gas void fraction, the contribution of the liquid phase in the mixture momentum equation becomes less important. Accordingly, at a high gas void fraction, the effect of liquid density on the vibrational frequencies is lower. From the graphical illustration, it can be concluded that the vibrational frequencies of the C-C system are higher than those of the P-P. Because the C-C boundary conditions have more constraints than the P-P, it can be concluded that the C-C system has a higher instability threshold than the P-P. Generally, choosing more restrained boundary conditions is an effective approach to improve the performance of systems conveying two-phase flow.

5. Conclusion

Based on the drift-flux two-phase model, linear and nonlinear free vibrations of pipes with both immovable ends were analyzed in detail by considering the effects of gravitational force, structural, and two-phase damping. The dynamical equation of the system was discretized with the help of the Galerkin approach, and linear vibrational frequencies were acquired. The closed-form expression for the nonlinear vibrational frequency of the system was also obtained. The model validation was conducted with the published numerical, analytical, and experimental results. The effects of flow parameters, geometrical and physical properties on the vibrational behavior of the system were examined in different flow regimes. The most important results of the present study can be summarized as follows:

- ✓ Among the bubbly, finely dispersed bubbly, and churn flow regimes, the system has the highest and lowest vibrational frequencies for churn and finely dispersed bubbly flow regimes, respectively.
- ✓ The two-phase damping effect leads to the decrement of the linear vibrational frequency of the system.
- ✓ Variation of flow parameters near the flow pattern transition boundaries has the greatest effect on the system dynamics.
- ✓ Compared with the two-phase damping effect, the hysteresis damping has a tangible impact on the linear vibrational frequency.

- ✓ Increasing the gas void fraction leads to the increment of vibrational frequencies.
- ✓ By increasing the flow mixture velocity, vibrational frequencies decrease gradually.
- ✓ Compared with decreasing effect of flow mixture velocity on the vibrational frequencies, the increasing effect of the gas void fraction is dominant.
- ✓ Pipes with the downward flow have higher vibrational frequencies than the upward.
- ✓ The vibrational frequencies are directly related to the length and outer diameter of the pipe.
- ✓ Flow parameters have the same effect on the linear and nonlinear vibrational frequencies of the system.
- ✓ The vibrational frequencies and stability of the system decrease by increasing the liquid density.
- ✓ The nonlinear vibrational frequency of the system is higher than the linear one.
- ✓ The difference between linear and nonlinear vibrational frequencies increases by variation of initial vibrational amplitude, geometric and physical properties of the system.

CRediT authorship contribution statement

Ali Ebrahimi-Mamaghani: Methodology, Software, Validation, Formal analysis, Formal analysis, Investigation, Writing – original draft. **Navid Mostoufi:** Resources, Writing – review & editing. **Rahmat Sotudeh-Gharebagh:** Conceptualization, Funding acquisition. **Reza Zarghami:** Conceptualization, Supervision.

Declaration of competing interest

The authors declare that they have no known competing financial interests or personal relationships that could have appeared to influence the work reported in this paper.

Acknowledgment

The Iran National Science Foundation (INSF) is acknowledged for postdoctoral fellowship granted to Dr. Ali Ebrahimi-Mamaghani (INSF-Grant No. 97009741).

References

- Adegoke, A.S., Oyediran, A.A., 2018. Natural frequencies, modes and critical velocities of top tensioned cantilever pipes conveying pressurized steady two-phase flow under thermal loading. *Research on Engineering Structures and Materials* 4, 297.
- An, C., Su, J., 2015. Dynamic behavior of pipes conveying gas-liquid two-phase flow. *Nucl. Eng. Des.* 292, 204–212.
- Bahaadini, R., Dashtbayazi, M.R., Hosseini, M., Khalili-Parizi, Z., 2018. Stability analysis of composite thin-walled pipes conveying fluid. *Ocean Eng.* 160, 311–323.
- Bamidele, O.E., Ahmed, W.H., Hassan, M., 2019. Two-phase flow induced vibration of piping structure with flow restricting orifices. *Int. J. Multiphas. Flow* 113, 59–70.
- Bhagwat, S.M., Ghajar, A.J., 2012. Similarities and differences in the flow patterns and void fraction in vertical upward and downward two phase flow. *Exp. Therm. Fluid Sci.* 39, 213–227.
- Bhagwat, S.M., Ghajar, A.J., 2014. A flow pattern independent drift flux model based void fraction correlation for a wide range of gas-liquid two phase flow. *Int. J. Multiphas. Flow* 59, 186–205.
- Bi, H.T., 2007. A critical review of the complex pressure fluctuation phenomenon in gas-solids fluidized beds. *Chem. Eng. Sci.* 62, 3473–3493.
- Carlucci, L., 1980. Damping and Hydrodynamic Mass of a Cylinder in Simulated Two-phase Flow.
- Carneiro, J., Fonseca Jr., R., Ortega, A., Chucuya, R., Nieckele, A., Azevedo, L., 2011. Statistical characterization of two-phase slug flow in a horizontal pipe. *J. Braz. Soc. Mech. Sci. Eng.* 33, 251–258.
- Charreton, C., Béguin, C., Ross, A., Etienne, S., Pettigrew, M., 2015. Two-phase damping for internal flow: physical mechanism and effect of excitation parameters. *J. Fluid Struct.* 56, 56–74.
- Ebrahimi-Mamaghani, A.E., Khadem, S., Bab, S., 2016. Vibration control of a pipe conveying fluid under external periodic excitation using a nonlinear energy sink. *Nonlinear Dynam.* 86, 1761–1795.
- Ebrahimi-Mamaghani, A., Sotudeh-Gharebagh, R., Zarghami, R., Mostoufi, N., 2019. Dynamics of two-phase flow in vertical pipes. *J. Fluid Struct.* 87, 150–173.

- Ebrahimi-Mamaghani, A., Sotudeh-Gharebagh, R., Zarghami, R., Mostoufi, N., 2020. Thermo-mechanical stability of axially graded Rayleigh pipes. *Mech. Base. Des. Struct. Mach.* 50 (2), 412–441.
- ElNajjar, J., Daneshmand, F., 2020. Stability of horizontal and vertical pipes conveying fluid under the effects of additional point masses and springs. *Ocean Eng.* 206, 106943.
- Goda, H., Hibiki, T., Kim, S., Ishii, M., Uhle, J., 2003. Drift-flux model for downward two-phase flow. *Int. J. Heat Mass Tran.* 46, 4835–4844.
- Gravelle, A., Ross, A., Pettigrew, M., Mureithi, N., 2007. Damping of tubes due to internal two-phase flow. *J. Fluid Struct.* 23, 447–462.
- Guo, R., Chen, Y., Waltrich, P.J., Williams, W.C., 2018. An experimental investigation on flow pattern map and drift-flux model for Co-Current upward liquid-gas two-phase flow in narrow annuli. *J. Nat. Gas Sci. Eng.* 51, 65–72.
- Hibiki, T., Ishii, M., 1998. Effect of flow-induced vibration on local flow parameters of two-phase flow. *Nucl. Eng. Des.* 185, 113–125.
- Hibiki, T., Ishii, M., 2003. One-dimensional drift-flux model for two-phase flow in a large diameter pipe. *Int. J. Heat Mass Tran.* 46, 1773–1790.
- Hibiki, T., Takamasa, T., Ishii, M., 2004. One-dimensional drift-flux model and constitutive equations for relative motion between phases in various two-phase flow regimes at microgravity conditions. In: International Conference on Nuclear Engineering, pp. 377–386.
- Holmes, P.J., 1977. Bifurcations to divergence and flutter in flow-induced oscillations: a finite dimensional analysis. *J. Sound Vib.* 53, 471–503.
- Ibrahim, R., 2011. Mechanics of pipes conveying fluids—part II: applications and fluidelastic problems. *J. Pressure Vessel Technol.* 133.
- Ishii, M., Mishima, K., 1984. Two-fluid model and hydrodynamic constitutive relations. *Nucl. Eng. Des.* 82, 107–126.
- Jamshidifar, H., Askari, H., Fidan, B., 2018. Parameter identification and adaptive control of carbon nanotube resonators. *Asian J. Control* 20, 1329–1338.
- Khudayarov, B., Komilova, K.M., Turaev, F.Z., 2019. The effect of two-parameter of Pasternak foundations on the oscillations of composite pipelines conveying gas-containing fluids. *Int. J. Pres. Pip.* 176, 103946.
- Li, F., An, C., Duan, M., Su, J., 2020. Combined damping model for dynamics and stability of a pipe conveying two-phase flow. *Ocean Eng.* 195, 106683.
- Liu, G., Wang, Y., 2018a. Natural frequency analysis of a cantilevered piping system conveying gas–liquid two-phase slug flow. *Chem. Eng. Res. Des.* 136, 564–580.
- Liu, G., Wang, Y., 2018b. Study on the natural frequencies of pipes conveying gas–liquid two-phase slug flow. *Int. J. Mech. Sci.* 141, 168–188.
- Lottati, I., Kornecki, A., 1986. The effect of an elastic foundation and of dissipative forces on the stability of fluid-conveying pipes. *J. Sound Vib.* 109, 327–338.
- Miwa, S., Mori, M., Hibiki, T., 2015. Two-phase flow induced vibration in piping systems. *Prog. Nucl. Energy* 78, 270–284.
- Monette, C., Pettigrew, M., 2004. Fluidelastic instability of flexible tubes subjected to two-phase internal flow. *J. Fluid Struct.* 19, 943–956.
- Montoya-Hernández, D., Vázquez-Hernández, A., Cuamatzi, R., Hernandez, M., 2014. Natural frequency analysis of a marine riser considering multiphase internal flow behavior. *Ocean Eng.* 92, 103–113.
- Mou, B., Bai, Y., 2018. Experimental investigation on shear behavior of steel beam-to-CFST column connections with irregular panel zone. *Eng. Struct.* 168, 487–504.
- Ni, Q., Zhang, Z., Wang, L., 2011. Application of the differential transformation method to vibration analysis of pipes conveying fluid. *Appl. Math. Comput.* 217, 7028–7038.
- Ortiz-Vidal, L.E., 2019. Effect of phase velocities prediction on fluidelastic instability of a cantilever pipe subjected to gas-liquid flow. In: ASME 2019 Pressure Vessels & Piping Conference.
- Osipov, A., Sin'kov, K., Sepsivtsev, P., 2014. Justification of the drift-flux model for two-phase flow in a circular pipe. *Fluid Dynam.* 49, 614–626.
- Oyelade, A.O., Oyediran, A.A., 2021. Nonlinear Dynamics of Horizontal Pipes Conveying Two Phase Flow. *European Journal of Mechanics-A/Solids*, 104367.
- Paidoussis, M.P., 1998. Fluid-structure Interactions: Slender Structures and Axial Flow, vol. 1. Academic press.
- Pettigrew, M., Taylor, C., 1994a. Two-phase flow-induced vibration: an overview (survey paper). *J. Pressure Vessel Technol.* 116, 233–253.
- Pettigrew, M., Taylor, C., 1994b. Two-phase Flow-Induced Vibration: an Overview (survey paper).
- Pirbadgh, T., Ahmadian, M., Fesanghary, M., 2009. On the homotopy analysis method for non-linear vibration of beams. *Mech. Res. Commun.* 36, 143–148.
- Ponte, P., Ritto, T., Deü, J.-F., 2020. Dynamic analysis of a pipe conveying a two-phase fluid considering uncertainties in the flow parameters. *J. Braz. Soc. Mech. Sci. Eng.* 42, 1–15.
- Roodgar Saffari, P., Fakhraie, M., Roudbari, M.A., 2020a. Free vibration problem of fluid-conveying double-walled boron nitride nanotubes via nonlocal strain gradient theory in thermal environment. *Mech. Base. Des. Struct. Mach.* 1–18. <https://doi.org/10.1080/15397734.2020.1819310>.
- Roodgar Saffari, P., Fakhraie, M., Roudbari, M.A., 2020b. Nonlinear vibration of fluid conveying cantilever nanotube resting on visco-pasternak foundation using non-local strain gradient theory. *Micro & Nano Lett.* 15, 181–186.
- Sheikhi, A., Sotudeh-Gharebagh, R., Alfi, M., Mostoufi, N., Zarghami, R., 2012. Hydrodynamic characterisation of liquid-solid two-phase fluidised beds: vibration signature and pressure fluctuations analyses. *Can. J. Chem. Eng.* 90, 1646–1653.
- Sheikhi, A., Sotudeh-Gharebagh, R., Zarghami, R., Mostoufi, N., Alfi, M., 2013. Understanding bubble hydrodynamics in bubble columns. *Exp. Therm. Fluid Sci.* 45, 63–74.
- Sun, J., Wang, Y., Liu, S., Dehghani, A., Xiang, X., Wei, J., et al., 2021. Mechanical, chemical and hydrothermal activation for waste glass reinforced cement. *Construct. Build. Mater.* 301, 124361.
- Taati, E., Borjalilou, V., Fallah, F., Ahmadian, M.T., 2020. On size-dependent nonlinear free vibration of carbon nanotube-reinforced beams based on the nonlocal elasticity theory: perturbation technique. *Mech. Base. Des. Struct. Mach.* 1–23. <https://doi.org/10.1080/15397734.2020.1772087>.
- Taitel, Y., Barnea, D., Dukler, A., 1980. Modelling flow pattern transitions for steady upward gas-liquid flow in vertical tubes. *AIChE J.* 26, 345–354.
- Tang, Y., Yang, T., 2018. Post-buckling behavior and nonlinear vibration analysis of a fluid-conveying pipe composed of functionally graded material. *Compos. Struct.* 185, 393–400.
- Wang, X., Lyu, X., 2021. Experimental study on vertical water entry of twin spheres side-by-side. *Ocean Eng.* 221, 108508.
- Wang, L., Yang, Y., Liu, C., Li, Y., Hu, Q., 2018. Numerical investigation of dynamic response of a pipeline-riser system caused by severe slugging flow. *Int. J. Pres. Pip.* 159, 15–27.
- Wiedemann, P., Döß, A., Schleicher, E., Hampel, U., 2019. Fuzzy flow pattern identification in horizontal air-water two-phase flow based on wire-mesh sensor data. *Int. J. Multiphas. Flow* 117, 153–162.
- Wu, H., Zhang, F., Zhang, Z., 2021. Droplet breakup and coalescence of an internal-mixing twin-fluid spray. *Phys. Fluids* 33, 013317.
- Xu, D., Liu, Q., Qin, Y., Chen, B., 2020. Analytical approach for crack identification of glass fiber reinforced polymer-sea sand concrete composite structures based on strain dissipations. *Struct. Health Monit.* <https://doi.org/10.1177/1475921720974290>.
- Ye, S.-Q., Ding, H., Wei, S., Ji, J.-C., Chen, L.-Q., 2021. Non-trivial equilibria and natural frequencies of a slightly curved pipe conveying supercritical fluid. *Ocean Eng.* 227, 108899.
- Zhang, C., Ali, A., 2021. The advancement of seismic isolation and energy dissipation mechanisms based on friction. *Soil Dynam. Earthq. Eng.* 146, 106746.
- Zhang, Y., Faghri, A., 2002. Heat transfer in a pulsating heat pipe with open end. *Int. J. Heat Mass Tran.* 45, 755–764.
- Zhu, H., Gao, Y., Zhao, H., 2019. Experimental investigation of slug flow-induced vibration of a flexible riser. *Ocean Eng.* 189, 106370.